minerals

MDPI

Article

Biomineralization and Characterization of Calcite and Vaterite Induced by the Fungus *Cladosporium* sp. YPLJS-14

Peilin Ye [1,2], Feirong Xiao [2] and Shiping Wei [1,2,*]

[1] Key Laboratory of Polar Geology and Marine Mineral Resources (China University of Geosciences, Beijing), Ministry of Education, Beijing 100083, China; peilinye1011@163.com
[2] School of Marine Sciences, China University of Geosciences, Beijing 100083, China; xfeirong@163.com
* Correspondence: weishiping@cugb.edu.cn

Abstract: Microbially induced calcium carbonate precipitation (MICP) by the urease-producing bacteria has wide applications in the field of geology and environmental engineering. Compared to bacteria, fungi usually possess more tolerance to high salts and heavy metals, enabling MICP induced by the urease-producing fungi to be applied to harsh environments. In this study, the carbonate minerals, induced by the urease-producing fungi isolated from marine sediments, were investigated. One of the urease-producing fungi, designated as YPLJS-14, was identified with the high efficiency of precipitating calcium carbonate. The ITS sequence of YPLJS-14 revealed that it belongs to the genus of *Cladosporium*. The precipitates induced by this strain were characterized by XRD, SEM, TEM, SAED, and FTIR, respectively. The results show that the mineral phase of fungal precipitates is composed of calcite and vaterite. SEM, TEM, and SAED confirm that the minerals in rhombohedral morphology are calcite and the spherical minerals are vaterite. Thermogravimetric and derivative thermogravimetric (TG/DTG) analyses show that vaterite is a thermodynamically unstable mineral phase compared to calcite and easily decomposes at lower temperatures. These findings provide a foundation for understanding the mineralization mechanism of the urease-producing fungi and the potential applications in environmental engineering.

Keywords: urease-producing fungi; biomineralization; microbially induced calcium carbonate precipitation (MICP); calcite; vaterite

Citation: Ye, P.; Xiao, F.; Wei, S. Biomineralization and Characterization of Calcite and Vaterite Induced by the Fungus *Cladosporium* sp. YPLJS-14. *Minerals* **2023**, *13*, 1344. https://doi.org/10.3390/min13101344

Academic Editors: Bin Lian, Hongchen Jiang and Yul Roh

Received: 23 September 2023
Revised: 15 October 2023
Accepted: 19 October 2023
Published: 22 October 2023

1. Introduction

Microbial mineralization is a common phenomenon in nature [1]. It can be categorized into three types based on the mechanisms of mineral formation: microbially induced, microbially influenced, and microbially controlled mineralization [2,3]. Out of these, microbially induced mineralization is widely observed in natural environments. This type of mineralization occurs outside of the microorganism cells, leading to a larger area of influence compared to other mechanisms. As a result, it holds potential applications in civil and environmental engineering, including carbon dioxide sequestration, the building structure repairs, heavy metal removal, and enhancement of concrete and soil performance [2,4–10].

Currently, our understanding of microbial-induced mineralization mainly relies on urease-producing bacteria. Those bacteria can break down urea into ammonia and carbon dioxide by producing urease during their metabolic processes. The increase in ammonia levels raises the pH of the surrounding environment, which triggers the reaction between Ca^{2+} and CO_3^{2-} to form calcium carbonate precipitation [10]. When bacteria induce the formation of calcium carbonate, three crystal phases are typically observed: calcite, aragonite, and vaterite. Calcite and vaterite are the most commonly observed polymorphs [2,8]. Bacteria-induced calcite often exhibits cubic, rhombic, and polyhedral morphologies [11] and is considered the thermodynamically most stable phase among the polymorphs of $CaCO_3$. In contrast, bacteria-induced vaterite has a hexagonal crystal structure and is

thermodynamically less stable compared to calcite. It has been reported that vaterite can transform into calcite under certain conditions [12]. Many factors may contribute to influencing the bacterial formation of different polymorphs of calcium carbonate minerals, including extracellular polymeric substances (EPSs), culture conditions (pH value), culture temperature, surface structure, and chemical properties of the bacterial strains [13–15]. However, the mechanism underlying the induction of vaterite formation by bacteria still requires further investigation.

Previous studies have shown that some fungi in nature also possess urease activities. They are often observed in the environments of soil, lakes, oceans, and forests [16–18], and they play a significant role in the nitrogen cycle in the ecological environments [19]. Given the remarkable ability of fungal hyphae to effectively penetrate and withstand harsh conditions [20], urease-producing fungi have great potential applications in areas such as self-healing concrete and bioremediation of heavy metals, etc. [16,21,22]. Similar to bacterially induced calcium carbonate precipitation, urease-producing fungi are also capable of inducing the formation of various calcium carbonate polymorphs. According to Li et al. [16], the precipitated calcium carbonate formed by *Neurospora crassa* during metal mineralization exclusively consisted of calcite. Menon et al. [23] utilized the urease-producing fungus *Aspergillus nidulans* MAD1445 for self-healing of concrete cracks. They observed that the induced precipitate mainly consisted of irregularly shaped calcite. Qian et al. [17] conducted a study on the removal of chromium and lead from water using carbonate mineralization by *Penicillium chrysogenum* CS1. They observed that the induced carbonate minerals primarily comprised rhombohedral calcite, with a minor presence of spherical vaterite. Indeed, the fungal formation of different calcium carbonate polymorphs, similar to bacteria, is still a subject of scientific investigation and exploration. The underlying mechanisms and processes involved in the specific mineral polymorph selection are not yet fully understood, and further research is needed to unravel this mystery.

Previous investigations have shown that marine fungi are widely distributed in marine habitats, with a variety of marine fungi frequently isolated from these environments [24]. In this study, the urease-producing fungus, *Cladosporium* sp., was isolated from the marine sediments. It aims to investigate the morphology, mineral characteristics, and thermodynamic properties of the calcium carbonate crystals induced by the fungus. It provides insights into the fungal biomineralization mechanisms. This knowledge can potentially pave the way for future applications of these fungi in marine carbon capture and storage by converting the carbon dioxide into carbonate minerals alongside various other applications in environmental remediation.

2. Materials and Methods

2.1. Isolation of Fungal Strains from Marine Sediments

The fungi were isolated from the marine sediment collected in Yancheng, Jiangsu Province, China (120.13° E, 33.38° N). Five grams of marine sediment was mixed thoroughly with 45 mL of sterilized water. Then, the suspension was made a ten-fold serial dilution up to 10^{-5}, and 100 µL of each dilution was spread on the rose bengal agar media [25] (g/L) (peptone 5, glucose 10, KH_2PO_4 1, $MgSO_4$ 1, rose bengal 0.033 and chloramphenicol 0.1, agar 20). The plates were incubated at 30 °C for 3–5 days until single colonies appeared. The single colonies were picked up and then transferred to the PDA media (g/L) (potato 200, glucose 20, agar 20) to obtain their pure cultures after incubation at 30 °C for 5 days (Figure 1). The fungal pure cultures were preserved in 20% glycerol and stored at −80 °C for the following experiments.

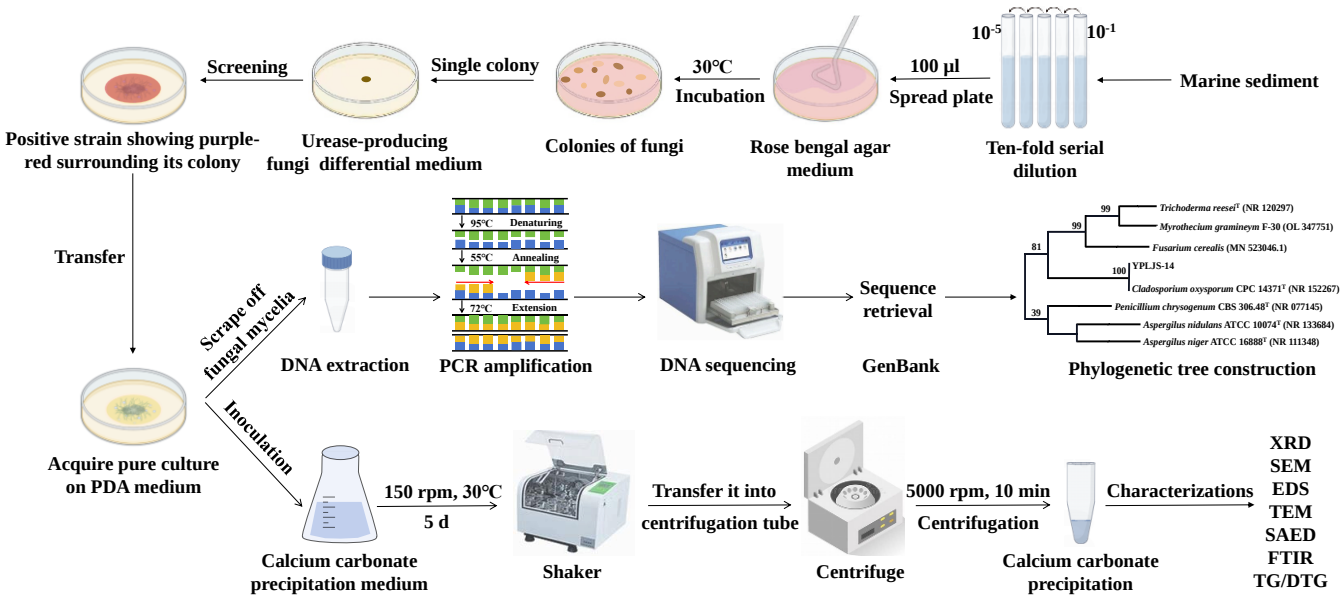

Figure 1. Illustration of isolation and identification of urease-producing fungi, preparation and collection of calcium carbonate precipitation, and mineral characterizations.

2.2. Screening and Identification of the Urease-Producing Fungi

The isolated fungi were inoculated on the media (g/L) (peptone 1, NaCl 5, glucose 1, KH_2PO_4 2, phenol red 0.012, urea, 20, agar 15, pH of 6.8) to screen and identify the urease-producing fungi. After 3–5 days of incubation at 30 °C, the medium color change from yellow to purple-red surrounding the fungal colonies indicated the candidate of urease-producing fungi (Figure 1).

The urease-producing fungi were inoculated on the PDA agar plates and incubated at 30 °C for 5 days. Approximately 0.1 g of fungal spores and mycelia was scraped off and added to a sterilized 1.5 mL centrifuge tube to extract its genomic DNA following the manufacturer's instructions (Invitrogen, Waltham, MA, USA). The Polymerase Chain Reaction (PCR) amplification was performed using the primers ITS4 (5′-TCCTCCGCTTATTGATATGC-3′) and ITS5 (5′-GGAAGGTAAAAGTCAAGG-3′) targeting the fungal internal transcribed spacer (ITS) region. The subsequent PCR amplification procedure that followed was as described by Zarrin et al. [26]. The amplified products were purified and then sequenced. The fungal ITS sequences were blasted against the GenBank database (http://www.ncbi.nlm.nih.gov/genbank/, accessed on 17 August 2023) and the reference sequences with high similarity were selected to construct a phylogenetic tree using the MEGA10 software (Figure 1).

2.3. Preparation and Collection of the Calcium Carbonate Precipitation

The urease-producing fungi were inoculated on PDA plates and incubated at 30 °C for 3 days. A block of fungal colony in 1 cm diameter was removed and placed in a sterilized centrifuge tube. Two milliliters of sterilized water were added to wash off the mycelia and spores and then inoculated into a 250 mL liquid calcium carbonate precipitation medium [11] (g/L) (nutrient broth 3, urea 20, $NaHCO_3$ 2.12, NH_4Cl 10, $CaCl_2 \cdot 2H_2O$ 4.9, pH 7.2) in a 500 mL Erlenmeyer flask. After autoclaving, the medium was supplemented with a filter-sterilized urea.

The Erlenmeyer flask was shaken and incubated for 5 days at 150 rpm under 30 °C until the calcium carbonate precipitate was noticeable at the bottom of the flask. The culture was then centrifuged at 5000 rpm for 10 min to collect the precipitate (Figure 1). Subsequently, the precipitation was washed three times with sterilized water and allowed to air dried in a petri dish for further analysis.

2.4. X-ray Diffraction Analysis

The fungal precipitate was ground into powder with a mortar and pestle. An appropriate amount of the powder was filled in a quartz XRD sample holder. Then, it was gently pressed, and we smoothed the surface using a glass slide. Afterwards, it was leveled and subjected to X-ray diffraction analysis using a Bruker D8 ADVANCE instrument. The instrument was operated under the conditions of 40 kV, 40 mA, Cu target wavelength of 1.5406 Å, and 2θ scanning angle range from 20° to 70°. The obtained XRD pattern was used to perform phase retrieval and analysis using the JADE 6.5 software equipped with the ICDD PDF database.

2.5. Scanning Electron Microscopy (SEM), Transmission Electron Microscopy (TEM), and Selected Area Electron Diffraction (SAED)

SEM was used to observe the fungal precipitates' morphologies. The fungal precipitates were glued on the SEM stub by a carbon double-tape and sputtered by platinum to enhance its conductivity. The SEM stub was loaded in the scanning electron microscope (FEI Quanta 200 FEG) and operated at an accelerating voltage of 15 kV. The SEM images were taken at different magnifications. TEM observation was performed using FEI Tecnai G2 F30. The fungal precipitate was suspended in water and then dropped onto a TEM copper grid until it completely dried. The TEM copper grid was placed into the instrument and operated at an acceleration voltage of 300 kV. The different morphologies of fungal precipitation were identified, and then, we performed the elemental composition analysis using coupled energy-dispersive X-ray spectroscopy (EDS). The selected area electron diffraction (SAED) was used to acquire its crystal structure.

2.6. Fourier Transform Infrared Spectroscopy (FTIR)

The fungal precipitate was finely grounded and mixed with dried KBr powder at a ratio of 1:100. The mixture was then loaded into a mold and pressed into pellets. FTIR analysis was performed using a Nicolet Is10 FTIR spectrometer. The instrument was operated at a resolution of 4 cm^{-1}, and the FTIR spectrum was recorded from 4000 to 500 cm^{-1}.

2.7. Thermogravimetric and Derivative Thermogravimetric (TG/DTG) Analysis

Based on the results obtained from XRD, SEM, and SAED, it was identified that the rhombic mineral in the fungal precipitate is calcite, while the spherical mineral is vaterite. Two minerals were separated under a microscope for comparison of their thermodynamic characteristics. Ten milligrams of each calcite and vaterite were taken and placed in a thermogravimetric (TG) analyzer (STA 449 F3/F5) for their thermal stability analyses. The samples underwent heating from 30 to 900 °C with a heating rate of 10 °C per minute under an (argon) Ar atmosphere. The mass lost patterns were obtained with the heating-up temperature. The TG output signal was differentiated electronically to give a derivative thermogravimetric (DTG) curve, which accurately reflects the weight loss with the temperature.

3. Results

3.1. Isolation and Identification of the Urease-Producing Fungi

A total of 23 fungal strains were isolated from the marine sediments. They were inoculated on the urease-producing detection plates containing phenol red to screen the urease-producing strains. It was observed that four fungal strains—YPLJS-1, YPLJS-6, YPLJS-7 and YPLJS-14—produced a purple-red halo around their colonies, which indicates that the production of urease by those fungal strains has converted urea into ammonia, resulting in an elevated pH and thus leading to the phenol red color changing from yellow to purple-red. The observed purple-red regions of the media were checked using a pH indicator strip, and it shown that the pH values were all greater than 8.5.

The four fungal strains were inoculated into a liquid calcium carbonate precipitation medium to compare their efficiencies for the production of calcium carbonate. It was observed that the YPLJS-14 strain induced the formation of precipitates early and rapidly. In 1–2 days of cultivation, the formation of precipitates was visible at the bottom of the Erlenmeyer flask. By the end of a 5-day cultivation, the YPLJS-14 strain produced more precipitates than the other strains. It was indicated that the YPLJS-14 strain exhibits a higher efficiency in inducing precipitate formation and thus was selected for the following experiments.

The ITS sequence of YPLJS-14 was performed Blast search against the GenBank database on 17th August 2023. It shows high similarity with the ITS sequences of *Cladosporium colombiae* (NR 119729), *Cladosporium tenuissimum* (NR 119855), and *Cladosporium oxysporum* (NR 152267), respectively. The ITS phylogenetic tree revealed that YPLJS-14 clustered closely with *Cladosporium* species based on 97% identity, and it was distinct from other urease-producing fungi (Figure 2).

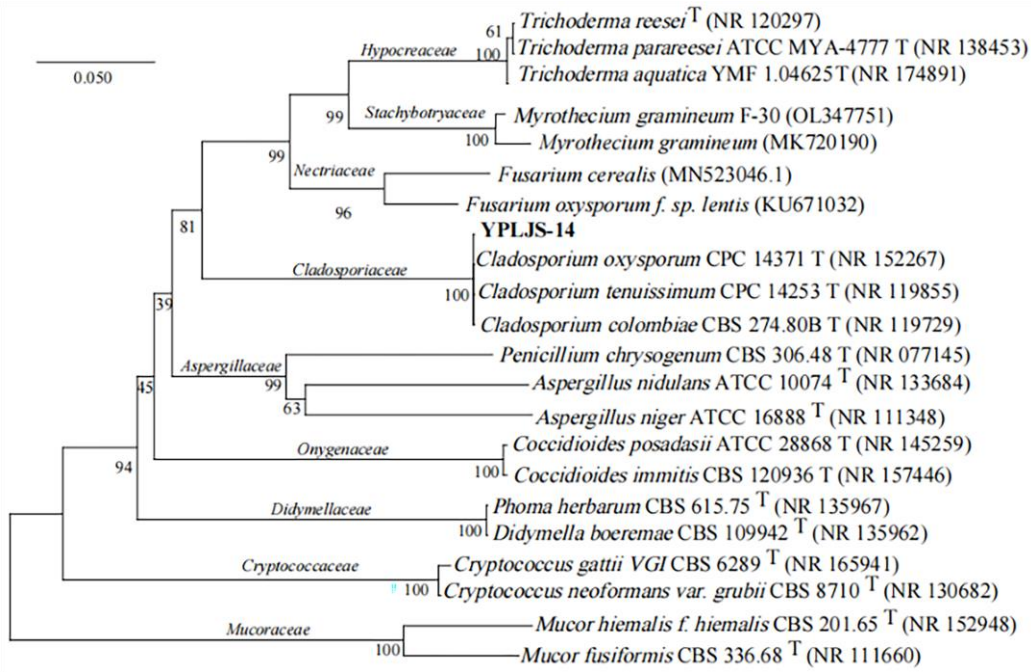

Figure 2. Phylogenetic tree of strain YPLJS-14 with the related species of urease-producing fungi based on ITS sequences. GenBank accession numbers are given in parentheses. The scale bar represents a 5% nucleotide sequence divergence.

3.2. Mineral Phase Analysis of the Fungal Crystals

The mineral phase of the fungal precipitate formed by YPLJS-14 was determined by XRD (Figure 3). The XRD spectrum showed that the peaks at 2θ angles of 23.059°, 29.409°, 35.975°, 39.417°, 43.166°, 47.125°, and 47.526° correspond to the crystal planes (012), (104), (110), (113), (202), (018), and (116) of calcite, according to the ICDD PDF standard card of calcite (PDF#83-0577). Additionally, the diffraction peaks at 2θ angles of 24.873°, 27.029°, 32.713°, 42.558°, 43.804°, 49.922°, and 51.027° are attributed to the crystal planes (110), (112), (114), (008), (300), (304), and (118) of vaterite (PDF#72-0506).

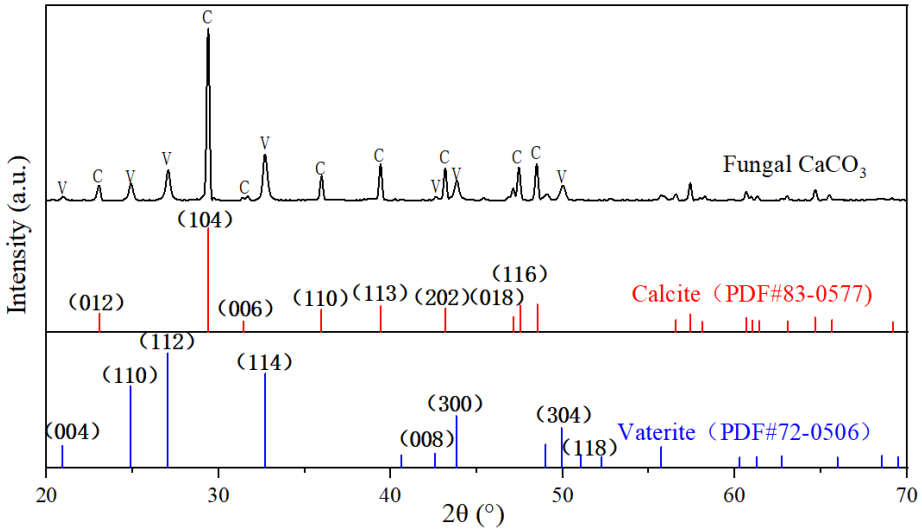

Figure 3. XRD pattern of the fungal precipitation formed by YPLJS-14.

To further determine the quantitative content of calcite and vaterite for the fungal precipitation formed by YPLJS-14, the XRD pattern of the sample was selected for performing Rietveld refinement. Figure 4 shows the observed (orange circles), calculated (black solid lines), difference (green lines), and Bragg positions (red short lines stand for the data of calcite with ICSD No. 20179, and blue short lines stand for the data of vaterite with ICSD No. 15879) results for the Rietveld refinement at room temperature. Table 1 depicts the crystallographic parameters of two phases of calcite and vaterite formed by YPLJS-14 as refined from X-ray powder diffraction. As shown in Figure 4 and Table 1, the refinement is stable and gives low R-factors (Rp = 3.76%, Rwp = 5.13% and χ^2 = 1.707), demonstrating the sample is composed of phase calcite and vaterite without any identified diffraction peaks from the impurity phase. The results show the weight percentage content of calcite and vaterite is 59.947 and 40.053 (Figure 4), respectively. The final refined results reveal a rhombohedral structure (space group R-3c) for calcite in the sample with the lattice parameters a = b = 4.9894 Å, c = 17.0872 Å, and V = 368.384 Å^3. These parameters are consistent with the standard data for calcite (ICSD no. 20179), where a = b = 4.9940 Å, c = 17.0810 Å, and V = 368.93 Å^3. Additionally, a hexagonal structure (space group P63/mmc) of vaterite is also identified with the lattice parameters a = b = 4.1013 Å, c = 8.4338 Å, and V = 122.856 Å^3, which is in agreement with the standard data for vaterite (ICSD no. 15879), where a = b = 4.1300 Å, c = 8.4900 Å, and V = 125.41 Å^3.

Table 1. Main parameters of the fungal calcite and vaterite refined from X-ray powder diffraction.

Phase	Calcite	Vaterite
space group	R-3c	P63/mmc
a (Å)	4.989401	4.1013
b (Å)	4.989401	4.1013
c (Å)	17.08729	8.433808
α (°)	90	90
β (°)	90	90
γ (°)	120	120
V (Å^3)	368.384	122.856
Rwp (%)	5.13	5.13
Rp (%)	3.76	3.76
Rexp (%)	3.93	3.93
χ^2	1.707	1.707
GoF	1.307	1.307

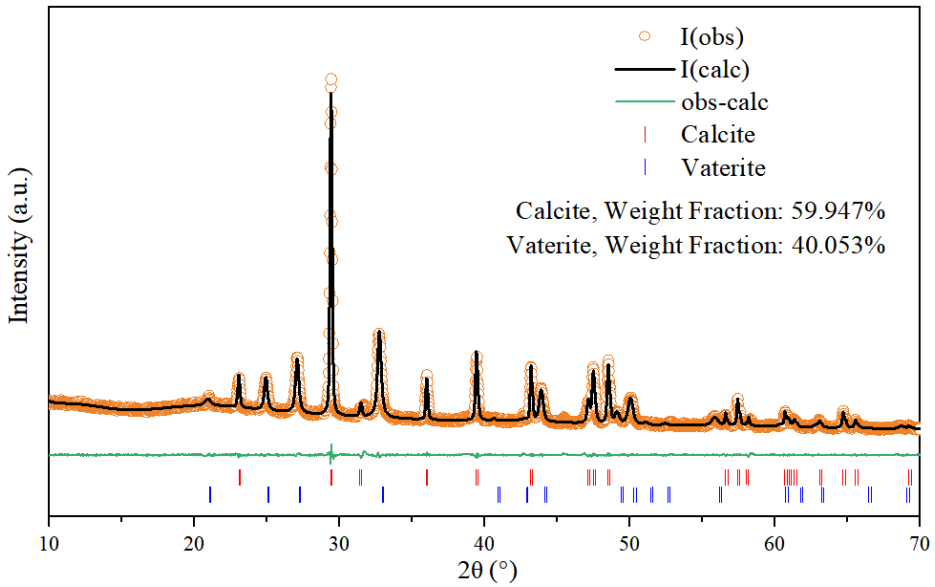

Figure 4. Rietveld refinement XRD pattern for the fungal calcite and vaterite. The observed (organ circles), calculated (black solid lines), difference (green lines), and Bragg positions (red short lines stand for the data of calcite with ICSD no. 20179, and blue short lines stand for the data of vaterite with ICSD no. 15879) results for the Rietveld refinement at room temperature.

3.3. Morphology and Elemental Characteristics of the Fungal Minerals

Morphologies of the fungal calcium carbonate were observed by SEM. Two types of minerals, the rhombohedral and the spherical, were dominantly observed in the fungal-formed minerals. In addition, an irregular morphology of minerals was also occasionally observed (Figure 5A,B). To distinguish the mineral phases of the rhombohedral and spherical minerals, the SAED patterns of each type mineral were acquired (Figure 5C,D). It reveals that the rhombohedral minerals belong to the trigonal crystal system with a rhombohedral crystal structure (Figure 5C). The spherical mineral belonged to the hexagonal crystal system, with a monoclinic crystal structure (Figure 5D). The SAED patterns combined with the XRD results (Figure 3) demonstrate that the rhombohedral mineral is calcite, while the spherical mineral is vaterite in the fungal precipitates. EDS was conducted on those two types of minerals for the elemental analysis, which shows that both the two types of minerals were mainly composed of carbon (C), oxygen (O), and calcium (Ca) (Figure 5E,F). A trace amount of chlorine (Cl) was detected in the precipitates, which may be involved from the medium components, which indicates during the process of biomineral formation, the other elements from the environment were often precipitated along with the biominerals.

3.4. FTIR Characterization of the Fungal Minerals

The FTIR spectrum was performed to characterize the functional groups of the calcium carbonate precipitate formed by YPLJS-14 (Figure 6). The peaks at the wavenumbers of 1075 cm^{-1} (ν_1) and 1410 cm^{-1} (ν_3) are assigned to the symmetric and asymmetric stretching vibrations of the CO_3^{2-} group, respectively. The peaks at 875 cm^{-1} (ν_2) and 745 cm^{-1} or 712 cm^{-1} (ν_4) corresponded to the out-of-plane bending and in-plane bending vibrations of the CO_3^{2-} group [27,28]. The peak at 712 cm^{-1} was the typical feature of calcite, while the peaks at 745 cm^{-1} and 1075 cm^{-1} were the typical characteristic of vaterite [29,30]. Furthermore, the peaks observed at 3434 cm^{-1}, 2932–3050 cm^{-1}, and 1628 cm^{-1} were attributed to the stretching vibrations of O-H, C-H, and C=O bonds [27], respectively, indicating that a certain of organic molecules were involved in the fungal calcium carbonate when it was precipitated by the fungus.

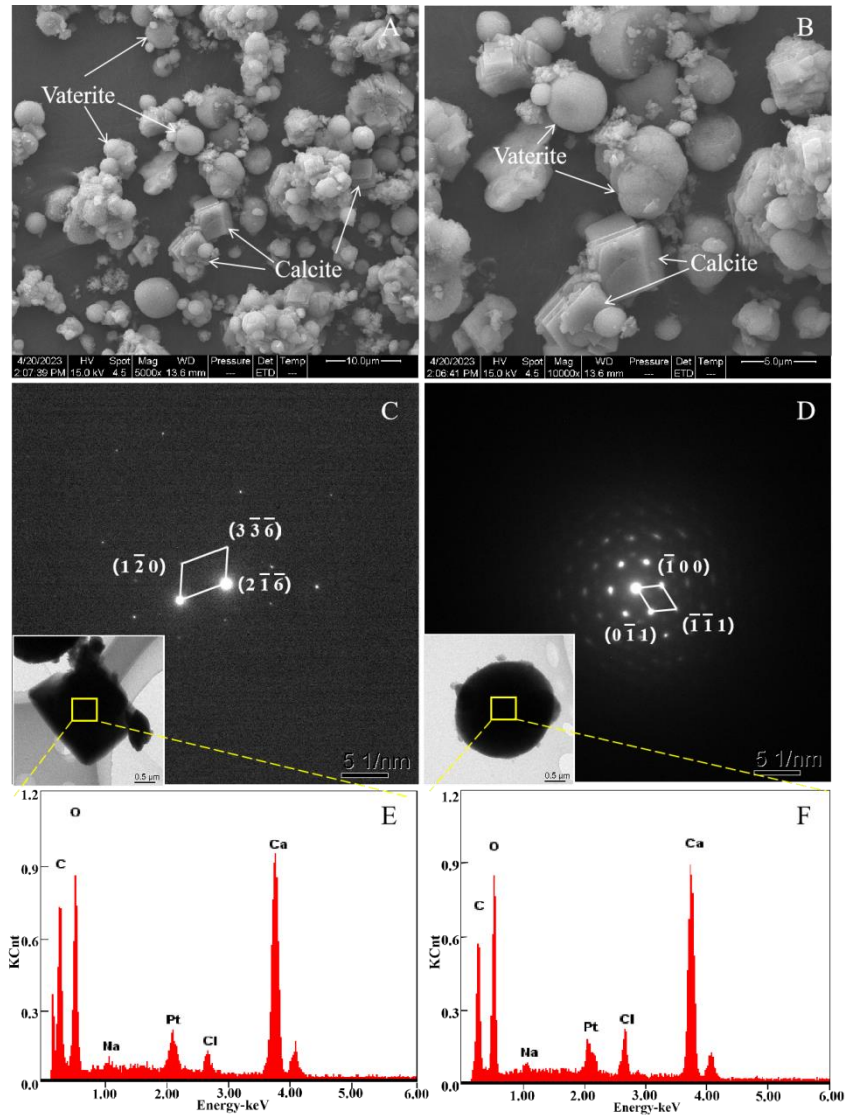

Figure 5. Characterization of the fungal minerals formed by YPLJS-14. (**A**,**B**), SEM; (**C**,**D**), SAED; (**E**,**F**), EDS; Insets in (**C**,**D**) show the TEM images of calcite and vaterite, respectively.

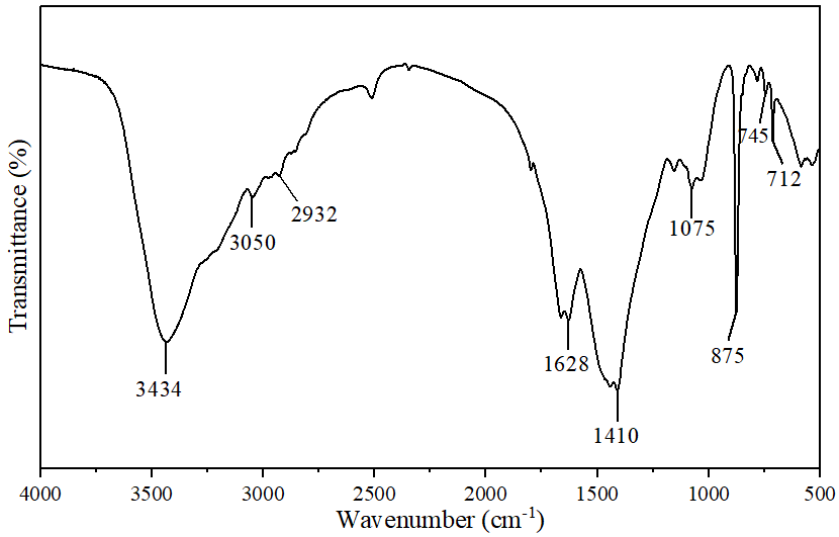

Figure 6. FTIR spectrum of the fungal-formed calcium carbonate.

3.5. TG/DTG Analysis of the Fungal Calcite and Vaterite

According to previous studies, calcite is the most thermodynamically stable polymorph among the calcium carbonate minerals, while vaterite is a metastable phase of calcium carbonate minerals. To compare the thermodynamic characteristics of these two minerals, the calcite and the vaterite were separated from each other in the mixture of fungal calcium carbonate minerals. Then, both of them performed the thermogravimetric (TG) and derivative thermogravimetric (DTG) analyses to determine their physical and chemical stability properties.

The results demonstrate that mass loss of calcite can be divided into two stages (Figure 7A). In the first stage of temperatures ranging from 30 to 593 °C, the mass loss accounts for 5%, which is caused by the adsorbed water in the calcite. The second stage of mass loss occurs between 593 and 794 °C, with a mass loss of 41%, which was attributed to the release of CO_2 during the decomposition of $CaCO_3$ into CaO. The DTG curve indicates that the fastest decomposition rate of calcite occurs at 752 °C. In contrast, the mass loss of vaterite can be divided into three stages (Figure 7B). The first mass loss occurs between 30 and 236 °C, with a mass loss of approximately 6.4%, which can be attributed to the physically adsorbed water in the vaterite. The second mass loss occurs between 236 and 603 °C, with a loss of approximately 12%, which is caused by the removal of crystalline water in the vaterite [31]. The third mass loss occurs between 603 and 794 °C, with a mass loss of approximately 29%, due to the removal of CO_2 from the vaterite [31]. Based on the DTG curve of vaterite, it is observed that the fastest decomposition rate of vaterite occurs at 735 °C, which is lower than that of calcite. This observation demonstrates the thermodynamic instability of vaterite compared to calcite.

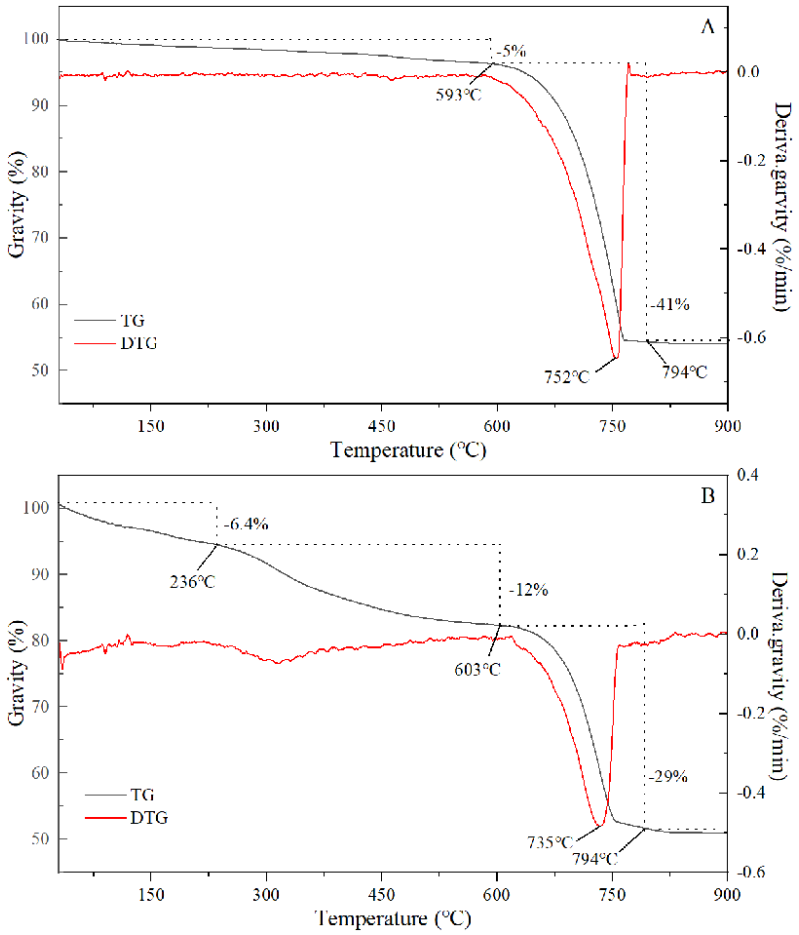

Figure 7. TG (black) and DTG (red) characterizations of the fungal calcite (**A**) and vaterite (**B**).

4. Discussion

4.1. Diversity of Urease-Producing Fungi

At present, the precipitation of calcium carbonate induced by urease-producing bacteria was extensively studied. In contrast, research on urease-producing fungi-induced calcium carbonate precipitation is relatively limited. Compared to bacteria, fungi often demonstrate higher tolerance to temperature, salt, and drought conditions [17,20,32]. Furthermore, the fungal mycelium can provide more nucleation sites during their mineralization processes [33,34], making them particularly significant in certain specific environments [23].

Previous studies have indicated that urease-producing fungi can be found in diverse environments, including soil, cement, and rocks [18,19,35]. Multiple species of urease-producing fungi have been isolated from those environments, including species belonging to the genera *Penicillium*, *Aspergillus*, *Fusarium*, *Mucor*, *Neurospora*, *Phoma*, *Cryptococcus*, *Coccidioides*, *Myrothecium*, and *Pestalotiopsis* [10,16,17,21,36–39]. In this study, we isolated a urease-producing fungus, YPLJS-14, from marine sediments, which belongs to the genus *Cladosporium*. Previous reports have shown that *Cladosporium* fungi are widely distributed and can be found in various environments such as soil, plants, food, and waste [40]. Alizadeh et al. [41] isolated a urease-producing fungus, *Cladosporium cladosporioides*, from a dairy pasture, which has an impact on urea decomposition in the soil, ultimately resulting in nitrogen loss. As of now, based on our knowledge, there are no reports available on the induction of calcium carbonate precipitation by *Cladosporium* species. Other genera of urease-producing fungi, such as *Neurospora crassa* [21], *Myrothecium gramineum* [16], *Penicillium chrysogenum* [17], *Aspergillus nidulans* [23], *Fusarium cerealis*, *Phoma herbarum*, and *Mucor hiemalis* [10], have been frequently reported that can induce calcium carbonate precipitation. These studies have provided evidence for the potential application of urease-producing fungi in concrete protection and heavy metal remediation.

4.2. Morphologies of Fungal Calcium Carbonate Minerals

The morphology of calcium carbonate minerals induced by urease-producing fungi varies greatly and often differs depending on the fungal strain. Menon et al. [23] discovered that the application of *Aspergillus nidulans* MAD1445 for the self-healing of concrete cracks resulted in the formation of calcium carbonate crystals, which were frequently observed as single blocks and plates that accumulated together. In a study conducted by Zhao et al. [10] investigating the protective effects of *Phoma herbarum* on cement, it was observed that the induced calcium carbonate crystals displayed a range of morphologies, including capsular, rosette-shaped, and irregular cylinders. Those morphologies were somewhat similar to those formed by *Pestalotiopsis* sp., which is a fungus isolated from calcareous soil. The calcium carbonate minerals formed by *Pestalotiopsis* sp. exhibited cubic, lamellar, and spherical structures. In contrast, *Mucor hiemalis* was found to typically produce irregular hexagonal prisms and spherical minerals [10], whereas *Myrothecium gramineum* predominantly formed minerals of spherical calcium carbonate [16]. In this study, it was found that the spherical minerals formed by *Cladosporium* sp. YPLJS-14 were highly similar to those formed by the aforementioned fungi. Moreover, *Cladosporium* sp. YPLJS-14 was also capable of producing rhombic and a small number of irregular calcium carbonate minerals. In a mineralization study conducted by Qian et al. [17] to remove chromate and lead from the liquid using *Penicillium chrysogenum* CS1, it was observed that an irregular layer of calcium carbonate often formed along the fungal hyphae, resulting in the formation of a dense thick shell. Over time, triangular pyramids and a few large rhombohedral crystals were also observed to develop. It was speculated that the organic macromolecules present on the fungal surface served as nucleation sites for calcium carbonate crystallization. These organic molecules are believed to play a significant role in influencing the morphology of the formed calcium carbonate minerals. In the chemical synthesis of $CaCO_3$ in vitro, the introduction of aspartic acid (Asp) into the system led to a transition of the synthesized calcium carbonate from cubic and rhombohedral forms to spherical forms [42]. This observation suggests that

the presence of organic molecules, such as aspartic acid, can influence the precipitation morphology of calcium carbonate. Thus, it is reasonable to speculate that the spherical calcium carbonate formed by *Cladosporium* sp. YPLJS-14 may contain biomacromolecules that contribute to the formation and stabilization of their morphology.

4.3. Minerals Phases of the Bacterial Formation of Calcium Carbonate

Calcite and aragonite are most commonly found as the two polymorphs of calcium carbonate in nature. They are widely distributed and can be found in various geological settings. In contrast, vaterite is less common and typically found in specific natural environments or formed by microorganisms in laboratory systems [43]. Previous studies have shown that the urease-producing fungi *Aspergillus nidulans* MAD1445 [23] and *Neurospora crassa* [21] can induce the precipitation of calcium carbonate, specifically in the form of calcite. However, Li et al. [16] observed that calcium carbonate precipitated by *Myrothecium gramineum* contained both calcite and vaterite phases. This finding is similar to our results, which showed two mineral phases of calcium carbonate formed by *Cladosporium* sp. YPLJS-14. Currently, our understanding of the mechanisms underlying the induction of different calcium carbonate polymorphs by urease-producing fungi is limited. Further research is needed to explore and elucidate the specific mechanisms and factors involved in this process. In contrast, research on the factors influencing the formation of different calcium carbonate polymorphs by bacteria has received more attention compared to urease-producing fungi. Numerous studies have focused on understanding the influence of factors such as strain, cell wall, extracellular structures, etc. [44] on the formation of different calcium carbonate polymorphs by bacteria. According to the study by Hoffmann et al. [45], the active groups present on the bacterial cell surface not only serve as nucleation sites for calcium carbonate precipitation but also influence or guide the formation of calcium carbonate minerals in different sizes, morphology, and crystalline phases. It was discoved by Ercole et al. [13] that the extracellular polysaccharides (EPS) of *Bacillus firmus* and *Bacillus sphaericus* played a role in promoting the formation of calcite. However, in a study conducted by Li et al. [46], it was discovered that the soluble low-molecular-weight EPS of *Shewanella piezotolerans* WP3 significantly promotes the formation of vaterite. Additionally, the cultivation conditions may also contribute to the formation of different calcium carbonate polymorphs by bacteria [47,48]. Overall, those findings from bacterial studies provide valuable clues for gaining further insight into the mechanisms underlying the formation of different calcium carbonate polymorphs by fungi.

4.4. Chemical Characteristics of Fungal-Induced Calcium Carbonate

The FTIR spectra of calcium carbonate induced by *Cladosporium* sp. YPLJS-14 revealed the peaks at 1410 cm^{-1}, 875 cm^{-1}, and 712 cm^{-1}, indicating the presence of calcite. This observation was consistent with the FTIR spectra of calcite formed by fungi *Pestalotiopsis* sp. [16], *Mucor hiemalis*, and *Fusarium cerealis* [10]. The presence of vaterite was identified based on the observation of peaks at 1075 cm^{-1} and 745 cm^{-1} [49]. Additionally, the peaks at 712 cm^{-1} and 745 cm^{-1} are commonly utilized to distinguish between calcite and vaterite [30]. Thus, it can be concluded that the calcium carbonate formed by *Cladosporium* sp. YPLJS-14 is predominantly composed of calcite and vaterite, which is also supported by XRD analysis. Furthermore, in the FTIR spectrum, the peaks observed at 3434 cm^{-1}, 2932–3050 cm^{-1}, and 1628 cm^{-1} were attributed to the vibrational modes of water molecules and organic functional groups. This is consistent with the general understanding that biominerals often incorporate organic molecules during their biomineralization processes [46,50,51].

Thermogravimetric analysis of the calcite and vaterite formed by *Cladosporium* sp. YPLJS-14 revealed that both of them experienced two to three weight loss events. However, only one of these events was attributed to the decomposition of $CaCO_3$, as shown in Figure 7. The decomposition temperatures for calcite and vaterite formed by *Cladosporium* sp. YPLJS-14 were approximately 752 °C and 735 °C, respectively. It suggests that the decomposition

temperature of vaterite is lower than that of calcite, indicating the instability of vaterite [52] due to its crystal structure [53]. Karunadasa et al. [54] conducted a study on the thermal stability of purified calcite and found that its decomposition occurred at a temperature of 790 °C. In a study conducted by Li et al. [55], calcium carbonate was synthesized by adding various organic acids to the system. This resulted in a decrease in the decomposition temperature from 792.8 to 783.4–787.9 °C, depending on the type of organic acid used. Siva et al. [31] added polyethylene glycol (PEG) to the system during the synthesis of calcium carbonate. They observed a decrease in the decomposition temperature of calcite, aragonite, and vaterite to a range of 650–750 °C. Those findings highlight the influence of organic molecules on the thermal stability of calcium carbonate. Based on those findings, it can be speculated that the fastest decomposition temperature of the calcite formed by *Cladosporium* sp. YPLJS-14 is lower than that of chemically synthesized calcite. This difference could be attributed to the presence of organic compounds during the fungal precipitation of calcite, which potentially affects its thermal stability. Saraya and Rokbaa [27] found that the addition of polysaccharides to the calcium carbonate synthesis system not only significantly promoted the formation of vaterite but also stabilized its morphology. This suggests that polysaccharides play an important role in controlling the crystal growth and morphology of calcium carbonate. However, the thermal stability of vaterite was relatively poor, with a decomposition temperature range of 671–680 °C. It suggests that the vaterite formed by *Cladosporium* sp. YPLJS-14 contains organic compounds, as indicated by FTIR analysis, which likely contribute to the decrease in its thermal stability. Further research is needed to identify and characterize the specific organic compounds that play an important role in stabilizing the morphology of calcium carbonate and influencing its thermal stability. However, Liu et al. [56,57] observed that vaterite containing organics, produced by *Bacillus subtilis* and *Bacillus velezensis*, exhibit a good stability when exposed to the temperatures below 300 °C. Furthermore, they exhibit remarkable resilience in the presence of water and various acid/base environments. These findings provide valuable insights into the potential use of *Cladosporium* sp. YPLJS-14 for long-term carbon sequestration and storage within the context of marine carbon fixation.

5. Conclusions

In this study, a urease-producing fungus belonging to the *Cladosporium* genus was isolated from marine sediments. This fungus demonstrated the formation of calcium carbonate in two distinct morphologies: rhombohedral and spherical. The rhombohedral morphology, which corresponds to calcite, represents a thermodynamically stable and relatively stable mineral phase among the different polymorphs of calcium carbonate. The formation of spherical morphology corresponds to vaterite, and during the process of calcium carbonate formation, certain organic molecules may incorporate into the minerals and play an important role in stabilizing its morphology. The presence of organic molecules contributes to its thermodynamic instability, making it an unstable mineral phase among the different polymorphs of calcium carbonate. Studying fungal-induced mineralization offers a window into understanding how fungi produce specific calcium carbonate polymorphs, potentially opening doors to innovative methods for controlling and engineering these polymorphs for a wide range of applications.

Author Contributions: Conceptualization, S.W.; methodology, P.Y.; software, P.Y. and F.X.; validation, S.W. and P.Y.; formal analysis, P.Y., F.X. and S.W; investigation, P.Y. and F.X.; resources, P.Y.; data curation, P.Y.; writing—original draft preparation, P.Y.; writing—review and editing, S.W.; visualization, P.Y.; supervision, S.W.; project administration, S.W.; funding acquisition, S.W. All authors have read and agreed to the published version of the manuscript.

Funding: This research was funded by the National Natural Science Foundation of China (42272359) and the Chinese "111" project (B20011).

Data Availability Statement: Not applicable.

Acknowledgments: We thank Qingfeng Guo at China University of Geosciences in Beijing for his invaluable assistance in the analysis of XRD patterns.

Conflicts of Interest: The authors declare that they have no conflict of interest.

References

1. Boquet, E.; Boronat, A.; Ramo-Cormenzana, A. Production of calcite (calcium carbonate) crystals by soil bacteria is a general phenomenon. *Nature* **1973**, *246*, 5270529. [CrossRef]
2. Anbu, P.; Kang, C.H.; Shin, Y.J.; So, J.S. Formations of calcium carbonate minerals by bacteria and its multiple applications. *SpringerPlus* **2016**, *5*, 250. [CrossRef] [PubMed]
3. Görgen, S.; Benzerara, K.; Skouri-Panetc, F.; Gugger, M.; Chauvat, F.; Cassier-Chauvat, C. The diversity of molecular mechanisms of carbonate biomineralization by bacteria. *Discov. Mater.* **2021**, *1*, 2. [CrossRef]
4. Whiffin, V.S.; Van Paassen, L.A.; Harkes, M.P. Microbial carbonate precipitation as a soil improvement technique. *Geomicrobiol J.* **2007**, *24*, 417–423. [CrossRef]
5. Dejong, J.T.; Mortensen, B.M.; Martinez, B.C.; Nelson, D.C. Bio-mediated soil improvement. *J. Ecol. Eng.* **2010**, *36*, 197–210. [CrossRef]
6. Mitchell, A.C.; Diderikksen, K.; Spangler, L.H.; Cunningham, A.B.; Gerlach, R. Microbially enhanced carbon capture and storage by mineral-trapping and solubility-trapping. *Environ. Sci. Technol.* **2010**, *44*, 5270–5276. [CrossRef]
7. Abo-EI-Enein, S.A.; Ali, A.H.; Talkhan, F.N.; Abdel-Gawwad, H.A. Application of microbial biocementation to improve the physico-mechanical properties of cement mortar. *HBRC J.* **2013**, *9*, 36–40. [CrossRef]
8. Dhami, N.K.; Reddy, M.S.; Mukherjee, A. Biomineralization of calcium carbonates and their engineered applications: A review. *Front. Microbiol.* **2013**, *4*, 314. [CrossRef]
9. Castro-Alonso, M.J.; Montañez-Hernandez, L.E.; Sañchez-Munoz, M.A.; Franco, M.R.M.; Narayanasamy, R.; Balagurusamy, N. Microbially induced calcium carbonate precipitation (MICP) and its potential in bioconcrete: Microbiological and molecular concepts. *Front. Mater.* **2019**, *6*, 216. [CrossRef]
10. Zhao, J.Y.; Csetenyi, L.; Gadd, G.M. Fungal-induced $CaCO_3$ and $SrCO_3$ precipitation: A potential strategy for bioprotection of concrete. *Sci. Total Environ.* **2022**, *816*, 151501. [CrossRef]
11. Wei, S.P.; Cui, H.P.; Jiang, Z.L.; Liu, H.; He, H.; Fang, N.Q. Biomineralization processes of calcite induced by bacteria isolated from marine sediments. *Braz. J. Microbiol.* **2015**, *46*, 455–464. [CrossRef]
12. Spanos, N.; Koutsoukos, P.G. The transformation of vaterite to calcite: Effect of the conditions of the solutions in contact with the mineral phase. *J. Cryst. Growth* **1998**, *191*, 783–790. [CrossRef]
13. Ercole, C.; Cacchio, P.; Botta, A.L.; Centi, V.; Lepidi, A. Bacterially induced mineralization of calcium carbonate: The role of exopolysaccharides and capsular polysaccharides. *Microsc. Microanal.* **2007**, *13*, 42–50. [CrossRef]
14. Sarayu, K.; Iyer, N.R.; Murthy, A.R. Exploration on the biotechnological aspect of the bacteria for the production of the cementitious materials—A review. *Appl. Biochem. Biotechnol.* **2014**, *172*, 2308–2323. [CrossRef] [PubMed]
15. Seifan, M.; Samani, A.K.; Berenjian, A. New insights into the role of pH and aeration in the bacterial production of calcium carbonate ($CaCO_3$). *Appl. Microbiol. Biotechnol.* **2017**, *101*, 3131–3142. [CrossRef]
16. Li, Q.W.; Csetenyi, L.; Paton, G.I.; Gadd, G.M. $CaCO_3$ and $SrCO_3$ bioprecipitation by fungi isolation from calcareous soil. *Environ. Microbiol.* **2015**, *17*, 3082–3097. [CrossRef] [PubMed]
17. Qian, X.Y.; Fang, C.L.; Huang, M.S.; Achal, V. Characterization of fungal-mediated carbonate precipitation in the biomineralization of chromate and lead from an aqueous solution and soil. *J. Clean. Prod.* **2017**, *164*, 198–208. [CrossRef]
18. Lu, Y.Y.; Chen, L.Z.; Yu, Q.Y.; Cheng, C.; Cheng, Y.J. *Fusarium oxysporum* induces mineralization recovery rare earth ions Lanthanum (III). *Acta Microbiol. Sin.* **2021**, *61*, 1621–1631.
19. Gadd, G.M. Geomycology: Biogeochemical transformations of rocks, minerals, metal and radionuclides by fungi, bioweathering and bioremediation. *Mycol. Res.* **2007**, *111*, 3–49. [CrossRef]
20. Luo, J.; Chen, X.B.; Crump, J.; Zhou, H.; Davies, D.G.; Zhou, G.W.; Zhang, N.; Jin, C. Interactions of fungi with concrete: Significant importance for bio-based self-healing concrete. *Constr. Build. Mater.* **2018**, *164*, 275–285. [CrossRef]
21. Li, Q.W.; Csetenyi, L.; Gadd, G.M. Biomineralization of metal carbonates by *Neurospora crassa*. *Environ. Sci. Technol.* **2014**, *48*, 1440–1446. [CrossRef]
22. Kumari, D.; Qian, X.Y.; Pan, X.L.; Achal, V.; Li, Q.W.; Gadd, G.M. Microbially-induced carbonate precipitation for immobilization of toxic metals. *Adv. Appl. Microbiol.* **2016**, *94*, 79–108. [PubMed]
23. Menon, R.R.; Luo, J.; Chen, X.B.; Zhou, H.; Liu, Z.Y.; Zhou, G.W.; Zhang, N.; Jin, C. Screening of fungi for potential application of self-healing concrete. *Sci. Rep.* **2019**, *9*, 2075. [CrossRef] [PubMed]
24. Zvereva, L.V.; Borzykh, O.G. Fungi in deep-sea ecosystems of the world ocean: A review. *Russ. J. Mar. Biol.* **2022**, *48*, 139–148. [CrossRef]
25. Liao, H.M.; Zhang, L.Y.; Hu, X.S.; Liao, X.J. Effect of high pressure CO_2 and mild heat processing on natural microorganisms in apple juice. *Int. J. Food Microbiol.* **2010**, *137*, 81–87. [CrossRef]
26. Zarrin, M.; Ganj, F.; Faramarzi, S. Analysis of the rDNA internal transcribed spacer region of the *Fusarium* species by polymerase chain reaction-restriction fragment length polymorphism. *Biomed. Rep.* **2016**, *4*, 471–474. [CrossRef]

27. Saraya, M.E.S.I.; Rokbaa, H.H.A.L. Preparation of vaterite calcium carbonate in the form of spherical nano-size particles with the aid of polycarboxylate superplasticizer as a capping agent. *J. Nanomater.* **2016**, *4*, 44–51.
28. Zhu, Y.; Li, Y.; Ding, H.; Lu, A.; Li, Y.; Wang, C. Multifactor-controlled mid-infrared spectral and emission characteristic of carbonate minerals (MCO_3, M = Mg, Ca, Mn, Fe). *Phys. Chem. Miner.* **2021**, *48*, 15. [CrossRef]
29. Chakrabarty, D.; Mahapatra, S. Aragonite crystals with unconventional morphologies. *J. Mater. Chem.* **1999**, *9*, 2953–2957. [CrossRef]
30. Vagenas, N.V.; Gatsouli, A.; Kontoyannis, C.G. Quantitative analysis of synthetic calcium carbonate polymorphs using FT-IR spectroscopy. *Talanta* **2003**, *59*, 831–836. [CrossRef]
31. Siva, T.; Muralidharan, S.; Sathiyanarayanan, S.; Manikandan, E.; Jayachandran, M. Enhanced polymer induced precipitation of polymorphous in calcium carbonate: Calcite aragonite vaterite phases. *J. Inorg. Organomet. Polym.* **2017**, *27*, 770–778. [CrossRef]
32. He, Z.Q.; He, C.X.; Zhang, Z.B.; Zou, Z.R. Mechanism of plant salt tolerance enhanced by arbuscular. *Acta Bot. Boreal.* **2007**, *27*, 414–420.
33. Yuan, J.H.; Cao, J.L.; Yu, F.; Ma, J.; Zhang, D.; Tang, Y.J.; Zheng, J. Microbial biomanufacturer of metal/metallic nanomaterials and metabolic engineering: Design strategies, fundamental mechanisms, and future opportunities. *J. Mater. Chem. B* **2021**, *33*, 6491–6506. [CrossRef]
34. Sokol, N.W.; Slessarev, E.; Marschmann, G.L.; Nicolas, A.; Blazewicz, S.J.; Brodie, E.L.; Firestone, M.K.; Foley, M.M.; Hestrin, R.; Hungate, B.A.; et al. Life and death in the soil microbiome: How ecological processes influence biogeochemistry. *Nat. Rev. Microbiol.* **2022**, *20*, 415–430. [CrossRef]
35. Gadd, G.M. Metals, minerals and microbes: Geomicrobiology and bioremediation. *Microbiology* **2010**, *156*, 609–643. [CrossRef] [PubMed]
36. Creaser, E.H.; Porter, R.L. The purification of urease from *Aspergillus nidulans*. *Int. J. Biochem.* **1985**, *17*, 1339–1341. [CrossRef]
37. Smith, R.T.; King, A.D., Jr.; Goodman, N. Isolation and characterization of urease from *Aspergillus niger*. *J. Gen. Microbiol.* **1993**, *139*, 957–962. [CrossRef]
38. Navarathna, D.H.M.L.P.; Harris, S.D.; Roberts, D.D.; Nickerson, K.W. Evolutionary aspects of urea utilization by fungi. *Fems Yeast Res.* **2010**, *10*, 209. [CrossRef]
39. Kappaun, K.; Piovesan, A.R.; Carlini, C.R.; Ligabue-Braun, R. Uerease: Historical aspects, catalytic, and non-catalytic properties—A review. *J. Adv. Res.* **2018**, *13*, 3–17. [CrossRef]
40. Bensch, K.; Braun, U.; Groenewald, J.Z.; Crous, P.W. The genus *Cladosporium*. *Stud. Mycol.* **2012**, *72*, 1–401. [CrossRef]
41. Alizadeh, H.; Kandula, D.R.W.; Hampton, J.G.; Stewart, A.; Leung, D.W.M.; Edwards, Y.; Smith, C. Urease producing microorganisms under dairy pasture management in soils across New Zealand. *Geoderma Reg.* **2017**, *11*, 78–85. [CrossRef]
42. Kim, J.H.; Song, S.M.; Kim, J.M.; Kim, W.S.; Kim, I.H. $CaCO_3$ crystallization with feeding of aspartic acid. *Korean J. Chem. Eng.* **2010**, *27*, 1532–1537. [CrossRef]
43. Grasby, S.E. Naturally precipitating vaterite (μ-$CaCO_3$) spheres: Unusual carbonates formed in an extreme environment. *Geochim. Cosmochim. Acta* **2003**, *67*, 1659–1666. [CrossRef]
44. Hammes, F.; Boon, N.; de-Villiers, J.; Verstraete, W.; Siciliano, S.D. Strain-specific ureolytic microbial calcium carbonate precipitation. *Appl Environ. Microbiol.* **2003**, *69*, 4901–4909. [CrossRef]
45. Hoffmann, T.D.; Reeksting, B.J.; Gebhard, S. Bacteria-induced mineral precipitation: A mechanistic review. *Microbiology* **2021**, *167*, 001049. [CrossRef]
46. Li, H.; Yao, Q.Z.; Wang, F.P.; Huang, Y.R.; Fu, S.Q.; Zhou, G.T. Insights into the formation mechanism of vaterite mediated by a deep-sea bacterium *Shewanella piezotolerans* WP3. *Geochim. Cosmochim. Acta* **2019**, *256*, 35–48. [CrossRef]
47. Li, Q.; Zhang, B.; Ge, Q.; Yang, X. Calcium carbonate precipitation induced by calcifying bacteria in culture experiments: Influence of the medium on morphology and mineralogy. *Int. Biodeter. Biodegr.* **2018**, *134*, 83–92. [CrossRef]
48. Ekprasert, J.; Fongkaew, I.; Chainakun, P.; Kamangam, R.; Boonsuan, W. Investigating mechanical properties and biocement application of $CaCO_3$ precipitated by a newly-isolated *Lysinibacillus* sp. WH using artificial neural networks. *Sci. Rep.* **2020**, *10*, 16137. [CrossRef]
49. Lv, J.J.; Ma, F.; Li, F.C.; Zhang, C.H.; Chen, J.N. Vaterite induced by *Lysinibacillus* sp. GW-2 strain and its stability. *J. Struct. Biol.* **2017**, *200*, 97–105. [CrossRef]
50. Johnston, C.W.; Wyatt, M.A.; Li, X.; Ibrahim, A.; Shuster, J.; Southam, G.; Magarvey, N.A. Gold biomineralization by a metallophore from a gold-associated microbe. *Nat. Biotechnol.* **2014**, *9*, 241–243. [CrossRef]
51. Liu, H.L.; Liu, X.R.; Li, X.F.; Fu, Z.Y.; Lian, B. The molecular regulatory mechanisms of the bacteria involved in serpentine weathering coupled with carbonation. *Chem. Geol.* **2021**, *565*, 120069. [CrossRef]
52. Ogino, T.; Suzuki, T.; Sawada, K. The formation and transformation mechanism of calcium carbonate in water. *Geochim. Cosmochim. Acta* **1987**, *51*, 2757–2767. [CrossRef]
53. Shaikh, A.M. A new crystal growth form of vaterite, $CaCO_3$. *J. Appl. Crystallogr.* **1990**, *23*, 263–265. [CrossRef]
54. Karunadasa, K.S.P.; Manoratne, C.H.; Pitawala, H.M.T.G.A.; Rajapakse, R.M.G. Thermal decomposition of calcium carbonate (calcite polymorph) as examined by in-situ high-temperature X-ray powder diffraction. *J. Phys. Chem. Solids* **2019**, *134*, 21–28. [CrossRef]
55. Li, X.G.; Lv, Y.; Ma, B.G.; Wang, W.Q.; Jian, S.W. Decomposition kinetic characteristics of calcium carbonate containing organic acids by TGA. *Arab. J. Chem.* **2017**, *10*, S2534–S2538. [CrossRef]

56. Liu, R.L.; Huang, S.S.; Zhang, X.W.; Song, Y.S.; He, G.H.; Wang, Z.F.; Lian, B. Bio-mineralisation, characterization, and stability of calcium carbonate containing organic matter. *RSC Adv.* **2021**, *11*, 14415. [CrossRef]
57. Liu, H.L.; Huang, H.Y.; Nie, W.J.; Sun, M.L.; Li, X.F.; Lian, B. Facilitated mechanism of biological vaterite stability mediated by *Bacillus velezensis* and its secretions. *ACS Earth Space Chem.* **2023**. [CrossRef]